Research Square

Preprints are preliminary reports that have not undergone peer review.
They should not be considered conclusive, used to inform clinical practice,
or referenced by the media as validated information.

An investigation of springback of TC4 alloy by triple-layer sheet hot stamping and cold die quenching process

Lida Yu
Xiaoming Yang
yangxm@ncst.edu.cn

North China University of Science and Technology
Shengqiang Liu
Xiaomin Huang
Baoyu Wang
Hongchao Ji

Research Article

Keywords: TC4 alloy, THF process, Springback, FE numerical simulation, Microstructural evolution

Posted Date: March 9th, 2026

DOI: https://doi.org/10.21203/rs.3.rs-8974075/v1

License: This work is licensed under a Creative Commons Attribution 4.0 International License.
Read Full License

Version of Record: A version of this preprint was published at The International Journal of Advanced Manufacturing Technology on May 4th, 2026. See the published version at https://doi.org/10.1007/s00170-026-18137-y.

An investigation of springback of TC4 alloy by triple-layer sheet hot stamping and cold die quenching process

Lida Yu[1], Xiaoming Yang[1, *], Shengqiang Liu[1], Xiaomin Huang[1], Baoyu Wang[2,3], Hongchao Ji[1]

1. College of Mechanical Engineering, North China University of Science and Technology, Hebei Tangshan, 063210, China

2. School of Mechanical Engineering, University of Science and Technology Beijing, Beijing 100083, China

3. Beijing Key Laboratory of Metal Lightweight Forming Manufacturing, Beijing 100083, China

*Corresponding author: Xiaoming Yang

E-mail: yangxm@ncst.edu.cn (Xiaoming Yang)

Abstract: In this paper, the springback behaviors of TC4 alloy under triple-layer sheet hot stamping forming (THF) process is studied. To verify the springback control ability of the process, the U-shaped part experiments were conducted, and the effects of forming temperatures and quenching times on springback is revealed. A finite element (FE) model is established to study the deformation characteristics of U-shaped parts and the stress relaxation (SR) behavior during the quenching process. The springback control mechanism of THF is analyzed. Finally, the forming experiments of typical aviation parts were carried out to verify the feasibility of this process. The study showed that the simulation results were consistent with the experimental results. The springback angle from 2.67° of 750°C to 0.46° of 900°C in the THF process. Compared with the results obtained by single-layer sheet hot stamping forming (SHF) process, the springabck angle decreases by 83.06% at 900°C. Meanwhile, the affected is much more by the quenching time than SHF. The springback angle decreases from 0.58° of 30s to 0.24° of 60s at 850°C. The thermal insulation effect of THF makes the SR of the parts more sufficient in the process of quenching, and the residual stress is fully released. In addition, it is found that the neutral layer shift in the fillet area at the bottom of THF parts is relatively small and is more sensitive to the effect of forming temperature. According to the FE simulation and microstructure analysis, it is jointly revealed that

the inner and outer layers at the bottom fillet are close to the ideal state of tension-compression symmetry. The typical aviation parts have a high forming accuracy under THF processes. This research provides a new strategy for achieving high-precision forming of titanium alloy thin-walled parts in the aerospace industry.

Key words: TC4 alloy, THF process, Springback, FE numerical simulation, Microstructural evolution

1 Introduction

In the field of aerospace, titanium alloy is widely used because of its excellent properties[1-2]. However, at room temperature, it exhibits high strength and low ductility. After unloading, titanium alloy components are affected by residual stress and elastic recovery resulting in a low forming accuracy[3-5]. This phenomenon is widespread in the forming process of thin-walled sheets. Therefore, to ensure the high-precision and high-quality forming of titanium alloy thin-walled parts, it is crucial to study and control the springback behavior during the forming process.

Much research has been done on the springback problem. Regarding to the control of springback, scholars typically employ analytical methods to predict the springback behavior during bending processes[6], and modify mold dimensions or process parameters to achieve compensation. Jiang et al.[7] established a U-shaped prediction model and studied the thermodynamic behavior of aluminum materials during sheet forming and springback processes. By comparing the results of the cases, the accuracy can be verified. However, for complex structures, the establishment of analytical models becomes extremely cumbersome, and the analysis usually requires a large amount of computation. In view of this problem, scholars use numerical simulation and experimental methods to realize the prediction of complex structures[8-9]. Zhang et al.[10] revealed the mechanism of stress diffusion and locking effect caused by micro-pits during bending and springback processes through experiments and FE analysis. However, due to the structural characteristics of thin-walled parts, fluctuations in process parameters have a particularly significant impact on springback. Huang et al.[11] studied the effects of blank holder force and stamping speed on specimen springback. The study found that both a larger blank holder force and a smaller stamping speed can

reduce the springback angle of the part. For titanium alloys, Yang et al.[12] established a semi-analytical model for the V-shaped springback angle of TC4 alloy at high temperatures, predicting and analyzing the springback trend. The effect of process parameters on springback is investigated through experiments and FE simulations. Zong et al.[13] conducted bending tests on TC4 alloy from room temperature to 850℃. The research has found that the magnitude of springback are related to the punch radius and temperature. Ao et al.[14] and Shivaprasad et al.[15] separately investigated the effects of electrical pulse frequency, peak current, and current path on the springback of TC4 alloy. The study found that the springback angle decreases with the increase of frequency and peak current density. The larger electroplastic effect results in a significantly smaller springback when the current passes through the deformation area compared to when it passes through the entire specimen.

At present, the springback behavior of titanium alloy thin-walled parts has been extensively studied in various forming processes. The superplastic forming is a typical hot forming process for titanium alloys[16]. However, its actual formation requires small grain size[17], appropriate forming temperature[18], and low strain rate[19], which have significant limitations. The thermal creep forming is also a common forming technique. The residual stress during deformation can be eliminated through creep deformation at high temperatures and SR[20], effectively controlling the amount of springback[21]. At the present stage, this process method is primarily applied to large-scale components. Chen et al.[22] studied the formability of TA32 alloy under isothermal forming conditions. The results show that the coarsening of the internal structure and the oxidation of the surface appear obviously, although the formability of the sheet material is improved. Under this process, when the part dimension is large, the tools require a longer heating time. Alternatively, welding can also be used for segmented forming[23], but this greatly increases the difficulty of precision control[24]. Therefore, a manufacturing process for thin-walled parts that can simultaneously meet the requirements is necessary.

The high-temperature cold mold quenching (HFQ) holds a dominant position in manufacturing due to its high-efficiency and low-cost characteristics. However, during

traditional HFQ, there is significant heat loss in the sheet material during the transfer and forming processes. Liu et al.[25] discovered the temperature of titanium alloy sheet drops significantly during the forming process. However, titanium alloys are sensitive to temperature, and a significant temperature drop can affect its formability. After forming, it is highly prone to springback due to concentrated residual stress. Kopec et al.[26] studied the formability of TC4 titanium alloy and found that its formability would decrease with the serious loss of temperature. In view of this phenomenon and combined with the advantages of HFQ process. Yang et al.[27] proposed the adoption of a separable THF process. That is, two layers of steel sheets hold the titanium alloy sheet for heating, transferring and forming. The research has found that the formability of parts significantly improves after adopting the THF process. Zhou et al.[28] studied the interfacial heat transfer characteristics of THF. The research found that the use of two layers of steel sheets on top and bottom can maintain the temperature of the titanium alloy sheet at a higher level during HFQ compared with SHF. However, the springback behavior of titanium alloy sheets under this process is complex and has not yet been studied.

In this paper, the springback law and control ability of TC4 alloy were studied under the THF process. The control groups were set up for both SHF and THF processes. Through experiments and FE simulations, the effects of different forming temperatures and quenching times on the springback of U-shaped parts are studied. The springback mechanism of THF is elucidated in combination with the SR behavior during quenching pressure. The stress differences between the inner and outer layers of the two processes were discussed and analyzed. The shift of the neutral layer and the evolution of microstructure during the bending process were considered. Finally, the forming experiments were conducted on typical aviation parts to verify its reliability. This research provides an effective strategy for improving the high-precision and high-quality forming of thin-walled titanium alloy parts in the aerospace field.

2 Experimental materials and details

2.1 Materials

The TC4 alloy thin sheet with a thickness of 1.6mm is adopted in this article. In

addition, HS1500HC steel with a thickness of 1.4mm is adopted as the auxiliary sheet material. Fig.1 shows the initial microstructure of the TC4 alloy. In the microstructure image, there is no obvious concentrated color system, and the grain orientation is random. The low angle grain boundaries (LAGBs) accounted for 49.2%. The large grains are surrounded by many fine grains with an average grain size of 4.61μm. The texture strength is 9.36. Through the room-temperature tensile test, the tensile strength of TC4 alloy is 1069MPa and the elongation is 4.7%.

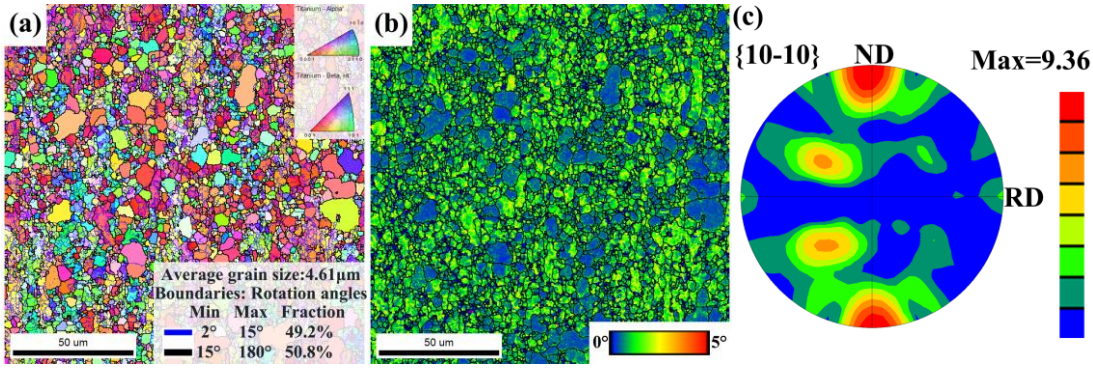


Fig.1 The initial microstructure of TC4 alloy: (a) Inverse pole figure + Grain boundary (IPF+GB) (b) Kernel average misorientation (KAM) (c) Pole figure (PF)

2.2 Experimental procedure for U-shaped parts

This paper conducted comparative experiments of SHF and THF respectively. The experimental equipment adopted is shown in Fig.2(a), mainly including a high temperature furnace, a hydraulic press and a control desk, among which the maximum pressure of the hydraulic press is 60T. The U-shaped tools were designed and manufactured, and installed on the hydraulic press, as shown in Fig.2(b). The tools are composed of top tool base, die, punch, blank holder plate, nitrogen gas spring, guide pillar and bottom tool base. During the forming and quenching process, the nitrogen gas spring supports the blank holder to provide the blank holder force for the sheet metal.

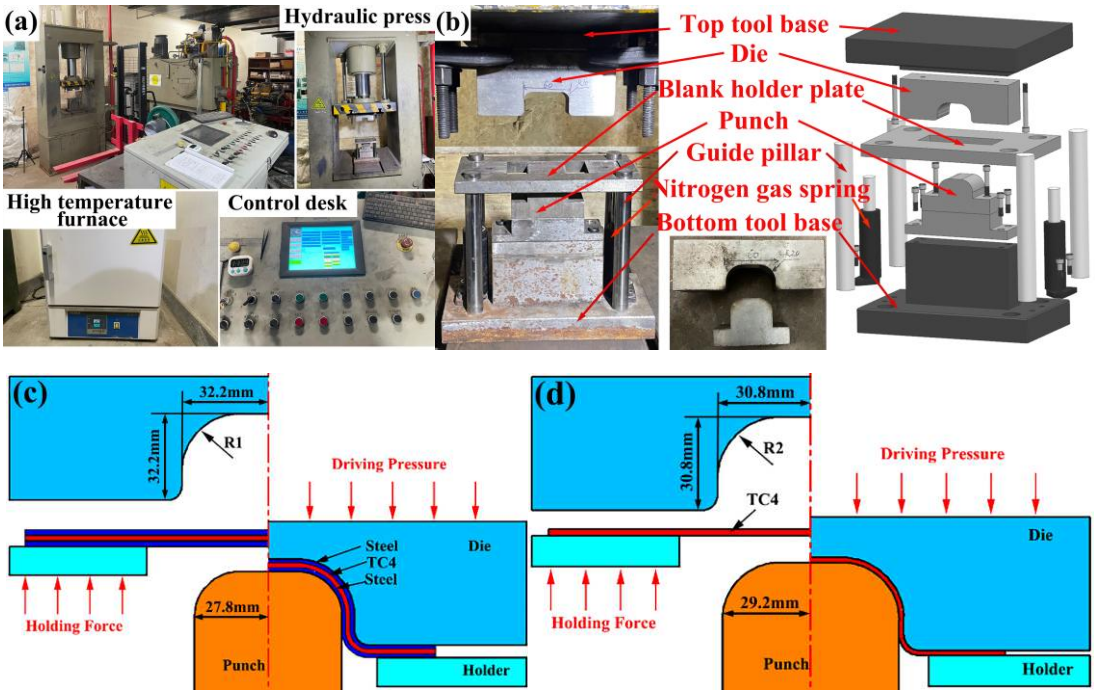


Fig.2 The experimental tools and forming principles: (a) Forming equipment (b) Forming tools (c) Forming principle of triple-layer (d) Forming principle of single-layer

Fig.2(c) and (d) respectively show the forming principles and tools dimension of SHF and THF. Among them, the THF is a titanium alloy sheet clamped by two layers of steel sheets for heating, transferring and forming. After HFQ is completed, the upper and lower steel parts are removed to obtain titanium alloy parts. Before the experiment began, the steel sheet and alloy titanium alloy sheet were cut into 180×50mm size samples by an electrical discharge wire cutting machine, with the length direction being the rolling direction. To prevent the surface of the sample from being oxidized, it is necessary to evenly apply high temperature antioxidant on its surface. During the experiment, the sheet metal sample is placed in a high temperature furnace for heating. Among them, the triple-layer sheets metal samples are directly placed in the order of steel-titanium alloy-steel. After the sheet metal is heated to the specified temperature, it is held at this temperature for 5 minutes before being removed and quickly transferred to the tool. The die moves downward to form the sheet metal, and quenching is carried out after the die is closed. Finally, the springback of the component is measured. The experimental scheme is shown in Table 1.

Table 1 Experimental scheme for U-shaped parts

Forming parameter	Value
Forming process	Triple-layer, Single-layer
Forming temperature/°C	750, 800, 850, 900
Quenching time/s	0, 10, 30, 60
Tool temperature/°C	25
Rounded corner radius of the part/mm	20
Blank holder force/KN	5
Stamping speed/mm·s^{-1}	30

3 FE simulation model

The springback FE models of titanium alloy U-shaped parts SHF and THF were established by using the simulation software Abaqus. Select half of the original size for modeling to improve computational efficiency. To ensure that the rounded corner radius of the formed titanium alloy parts is 20mm, the rounded corner radius sizes of the die and punch of the SHF and THF tools are shown in Fig.3. During the simulation process, a fixed blank holder force is applied upward on the blank holder plate, and the die moves downward to complete the die closing, while a fixed holding force is applied. After the force quenching is completed, the tools are removed and the parts freely springback to simulate the actual unloading process.

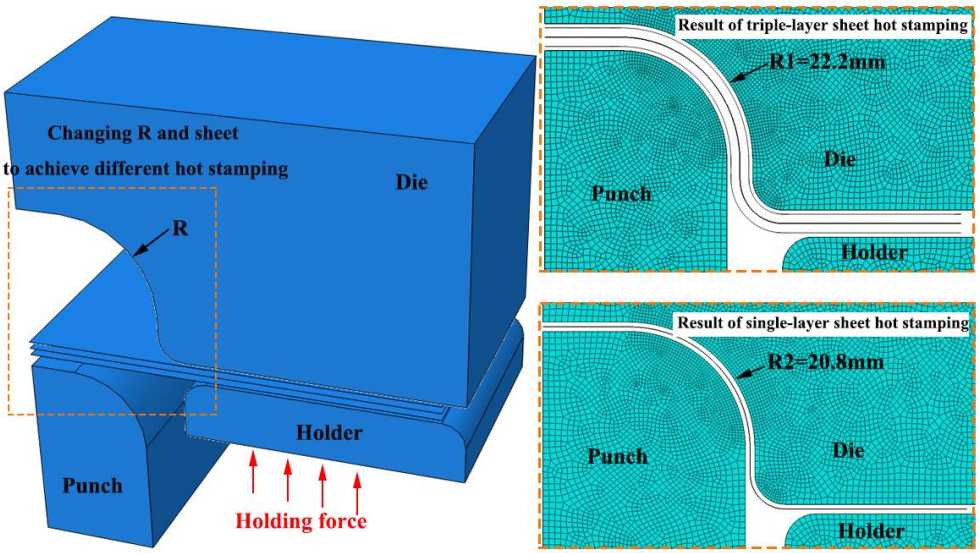


Fig.3 FE model of hot stamping process

In the FE model, the die, punch and blank holder plate are all divided into temperature-displacement coupled rigid body units C3D8T, and the initial temperature of the tool is 25°C. At the positions in contact with the sheet metal, the mesh is densified, as shown in Fig.3. The tool material is H13, and the steel sheet and titanium alloy sheet are HS1500HC and TC4, respectively. The thermal physical property parameters of the material are shown in Table 2[27]. The shell element S4RT with temperature-position coupling is adopted as the mesh type of the sheet metal, and the mesh is divided into 2mm. The Simpson Principle is adopted, and the thickness integration point is set to 5. Lang et al.[29]found that a larger friction coefficient between triple-layer sheets is conducive to improving the formability of the intermediate sheet material. Therefore, the friction coefficient between the sheets is set as 0.2[30]. The coefficient of friction between the sheet metal and the tools are set as 0.3. Fig.4 shows the stress-strain curves of TC4 alloy sheet and HS1500HC steel sheet.

Table 2 Thermal physical property parameters

Parameters		Values					
Temp(°C)		25	200	400	600	800	1000
Density(kg/m^3)	H13	7780	-	7640	7600	-	-
	Steel	7848	7790	7722	7644	7616	7519
	TC4	4500	-	-	-	-	-
Thermal conductivity (W/(m·K))	H13	36.5	29.9	29.2	28.3	27.5	-
	Steel	30.7	30	27.6	25.6	23.6	21.7
	TC4	6.95	8.87	10.5	12.9	15	17.4
Specific heat (J/(kg·K))	H13	440	510	548	590	640	-
	Steel	440	520	561	581	590	603
	TC4	612	652	691	712	720	725

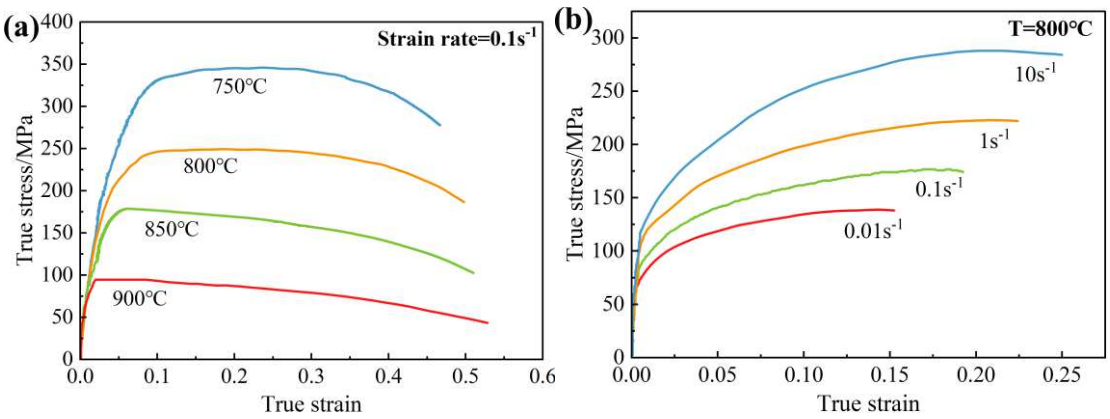


Fig.4 The stress-strain curves of experimental sheets: (a) TC4 alloy at $0.1s^{-1}$ (b) HS1500HC alloy at 800°C

4 Results and analysis

4.1 Experimental and simulation results

Fig.5(a) shows the springback results after unloading in the SHF and THF experiments. Both processes can obtain titanium alloy U-shaped parts with good forming effects, and no cracking occurs. Compared with the two processes, the former parts obtained by SHF show significant springback, while the parts of THF only exhibited significant springback under lower temperature conditions. When the forming temperature is 900°C, the springback of the formed part is significantly reduced. At 850°C, the temperature distribution of the formed parts under different quenching times is recorded by the thermal imager for the two processes, which is shown in Fig.5(b). The maximum temperature of SHF parts occurs at the top position, which is 165.16°C. After quenching for 30s, the position of the maximum temperature gradually shifted to the bottom rounded corner and dropped to 45.98°C. The maximum temperature of THF parts is 516.97°C, and the temperature distribution is uniform. After quenching for 30s, it still has 286.27°C. The cross-sectional profiles of the formed parts obtained from the experiment were obtained through a scanner, and the results are compared with the design size. Fig.5(c) and (d) show the cross-sectional profile of the formed parts after scanning by the two processes. As the temperature increases, the part size gets closer to the design size, the springback is smaller, and the forming effect is better.

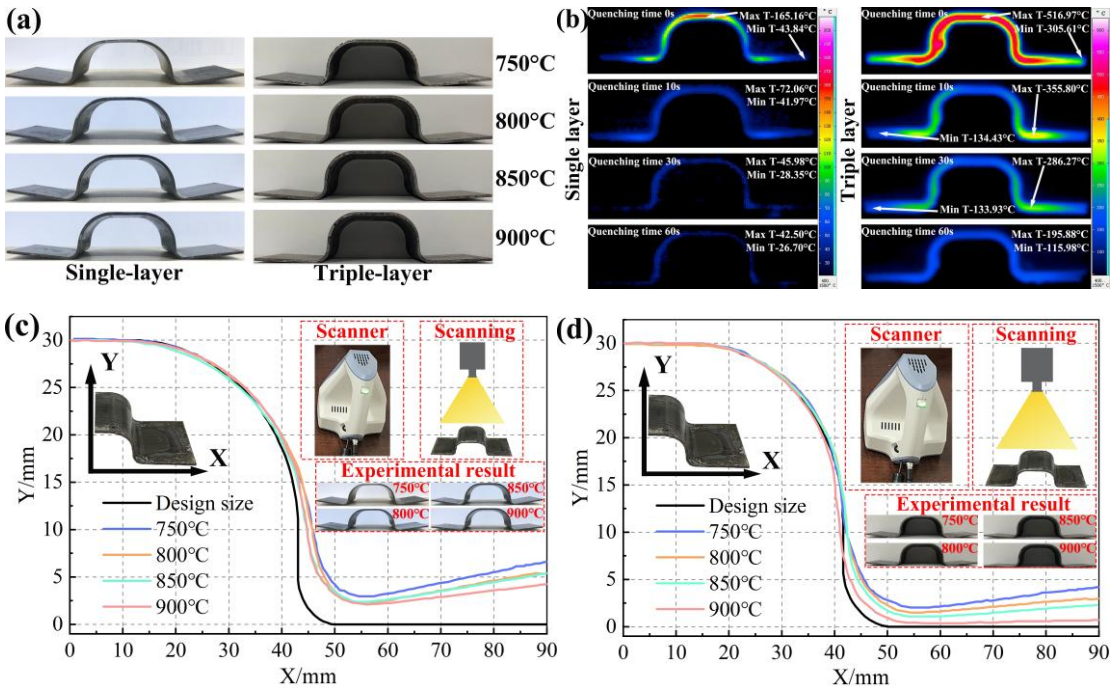


Fig.5 The experimental results: (a) U-shaped parts (b) The temperature distribution at different quenching times at 850℃ (c) Single-layer springback results contour curves (d) Triple-layer springback results contour curves

The forming of U-shaped parts can be divided into five areas to analyze, as shown in Fig.6(a). Among them, area I is in direct contact with the top of the punch, which can be regarded as maintaining a straight-line state. Area II and IV are the two fillets of the U-shaped part, which can be regarded as forward tension and bending forming. Area III is the side wall part of the U-shaped component. Area V is in direct contact with the blank holder and the bottom of the die, maintain a straight-line state during the forming process. After unloading, different areas of the sheet will have corresponding springback due to the deformation histories. During the quenching stage, the THF parts still have a higher temperature at area IV compared to the SHF parts. In view of this significant difference, this paper only measured the springback angle of the area IV.

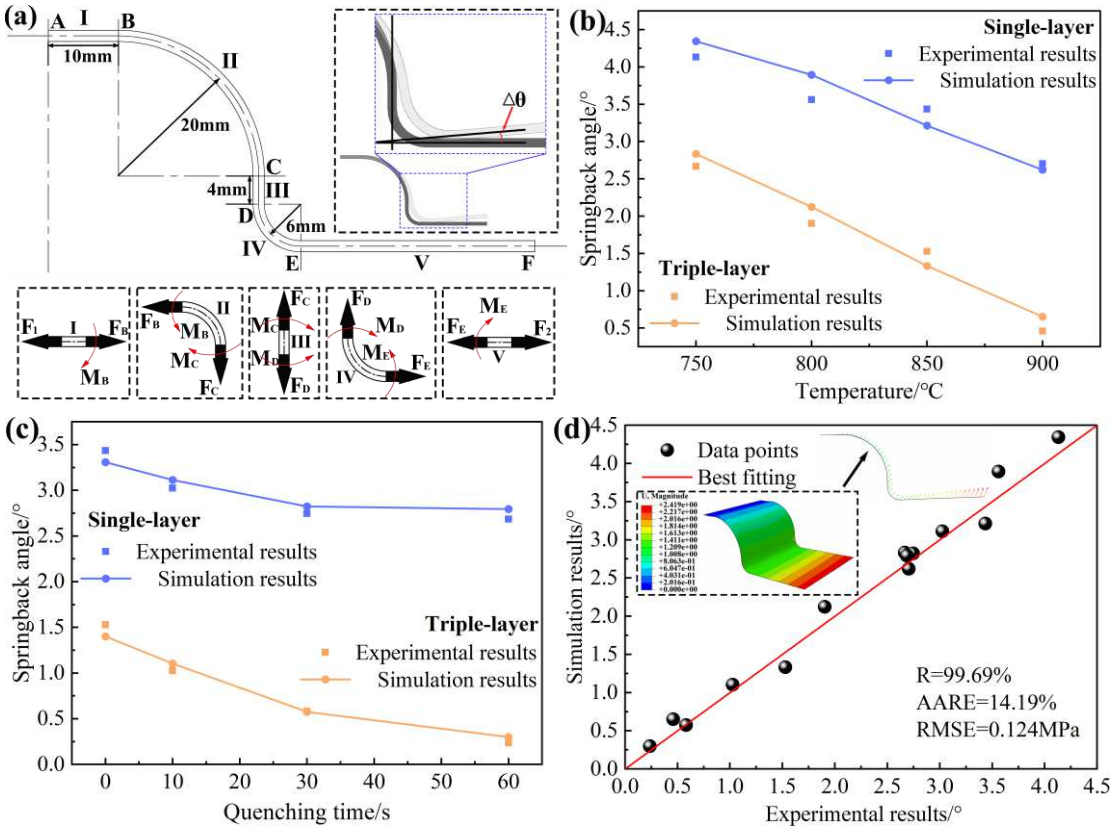


Fig.6 (a) Schematic diagram of U-shaped part bending (b) Springback comparison at different forming temperatures (c) Springback comparison of different quenching times at 850°C (d) Correlation analysis

Fig.6(b) and (c) shows the springback angle variations of the TC4 alloy parts in experiments and simulations under different forming conditions for the two processes. The springback angle of TC4 alloy sheet decreases with the temperature and quenching time increasing, and the springback angle is low in the THF process. The springback angle decreases from 2.67° of 750°C to 0.46° of 900°C in the THF process, which decreases by 82.78%. Compared with the results obtained by SHF process, the springabck angle decreases by 83.06% at 900°C. In the SHF process, the impact of quenching time on springback becomes less significant when the quenching time exceeds 30s. The springback angle decreases from 2.75° of 30s to 2.69° of 60s, which decreases by 2.18%. However, the influence of quenching time on springback remains significant when the quenching time exceeds 30s in the THF process. The springback angle decreases from 0.58° of 30s to 0.24° of 60s, which decreases by 58.62%. This is because that TC4 alloy sheet can retain more heat to facilitate SR after stamping in the

THF process. The residual stress and elastic deformation decrease with increasing quenching time due to the effect of SR. Therefore, the springback angle will continuously decrease with the quenching time increasing in the THF process.

To verify the predictive ability of the FE model, the linear correlation coefficient R, the average absolute relative error (AARE), and the root mean square error (RMSE) are used for evaluation[31]. Fig.6(d) shows the correlation analysis between the experimental and predicted results. The correlation coefficient R is 99.69%, AARE is 14.19%, and RMSE is 0.124MPa. The simulation prediction results have a good consistency with the experimental results.

4.2 Stress and strain distribution of TC4 alloy sheets

Fig.7(a) shows the stress distribution of parts after SHF and THF. The maximum stress of THF parts decreases from 310.5MPa at 750℃ to 255.3MPa at 900℃, which decreases by 17.8%. In addition, the stress of parts formed with THF at different forming temperatures is generally lower than that of SHF, and the distribution is more uniform., The parts of SHF showed obvious stress concentration at the junction of area IV and area V at 750℃ and 800℃. Higher concentrated stress will cause the unloaded parts to be more prone to springback due to the release of stress. This phenomenon is improved at 900℃. Under the effect of frictional resistance, a lower temperature makes the fluidity of the material worse. The phenomenon of excessive local stress and uneven distribution occurs. However, this phenomenon did not occur in the parts that adopted THF. Fig.7(b) shows the distribution of stress along the path at 850°C. Since the area III has undergone both forward tensile bending and reverse bending straightening, the stress in both processes is the highest here. The stress of the parts using THF is 279.7MPa, which is 41.2MPa lower than that of SHF at 320.9MPa. The stress of THF shows a trend of first decreasing and then increasing, and the variation curve is relatively smooth. However, SHF shows a tortuous upward trend with obvious fluctuations and relatively high stress.

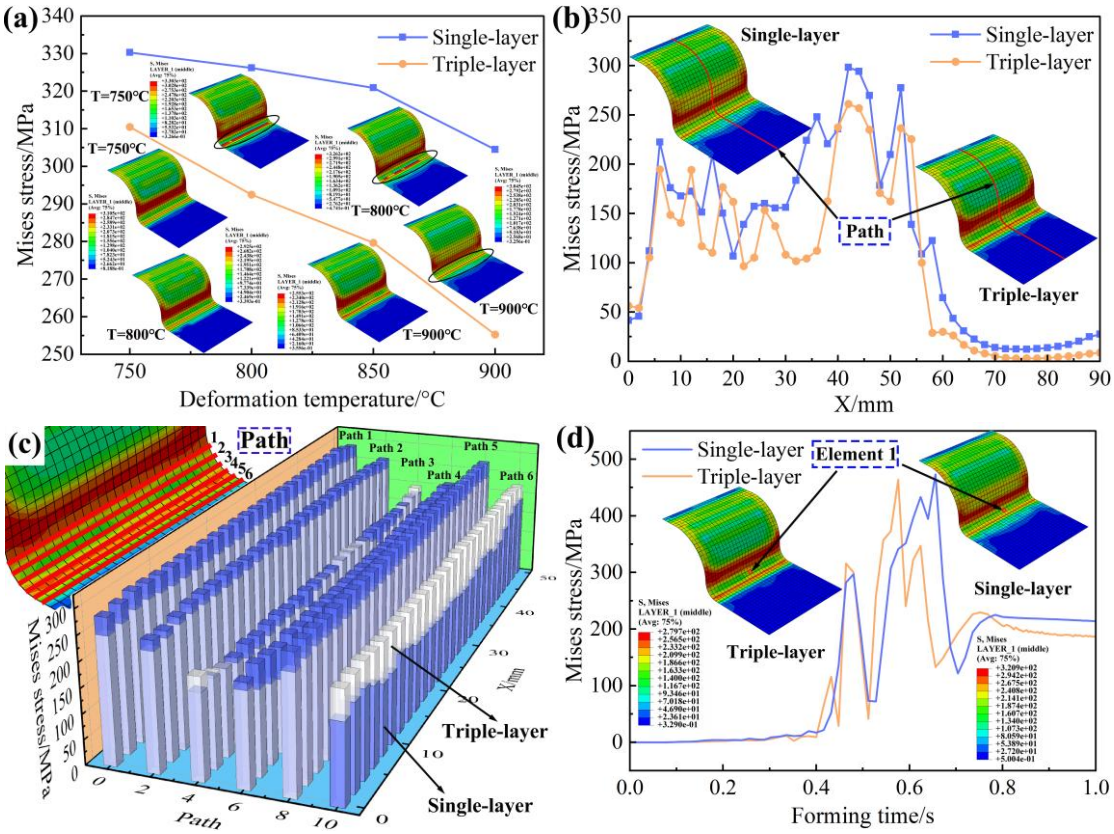


Fig.7 The stress distribution results: (a) Stress comparison (b) Stress distribution along the path at 850℃ (c) Stress distribution along the path in area IV at 850℃ (d) Stress changes during forming in area IV at 850℃

Fig.7(c) shows the stress distribution in area IV. The 3D graph can more intuitively show that the stress of SHF is higher than that of THF in the 0-8mm range. At 10mm, the stress of SHF is relatively low. This is because around 8-10mm is the junction of area IV and area V, and there is a stress concentration phenomenon at this position. The parts of THF are subjected to load transmission through steel sheets and titanium alloy sheets, resulting in a phenomenon of low stress and large area. The larger stress area extends beyond 10mm. However, SHF shows a phenomenon of high stress and small area, with obvious stress concentration. The stress changes of element 1 in area IV during the forming process are shown in Fig.7(d). The stress of THF changed earlier than expected after 0.5s, and the duration of its high-stress state is relatively short. This may be because of the deformation of the sheet in advance under THF. The SR phenomenon appears at high temperature, and the SR speed is faster.

Fig.8(a) shows the comparison of the equivalent plastic strain of the parts after

SHF and THF. the maximum strain of the parts using THF is in area III, which increases with the temperature increasing. The maximum strain of THF increased from 0.369 to 0.3749. As shown in Fig. 8(b), the equivalent plastic strain of the two processes is distributed along the path at 850℃. The maximum strain of THF is 0.3723, which is significantly greater than that of SHF at 0.3113. The larger plastic strain indicates that the elastic strain in the material is relatively small, and the possibility of springback after unloading is smaller. In addition, the large strain area is mainly distributed within the range of 30-45mm. Compared with SHF, its regional range is larger, and the strain variation curve along the path is gentler. A gentler strain variation also reduces the springback after unloading.

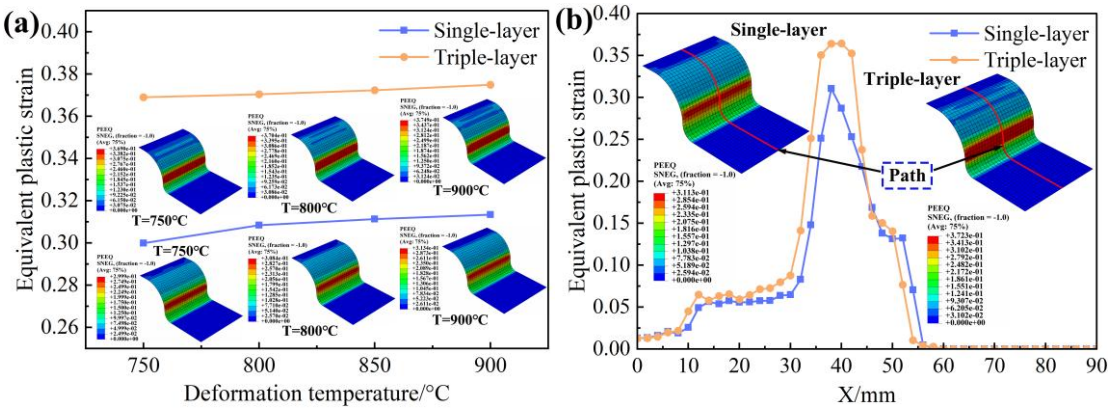


Fig.8 The equivalent plastic strain distribution results: (a) Strain comparison (b) Strain distribution along the path after forming at 850℃

4.3 Effect of temperature on springback

Fig.9(a) shows the comparison of part temperatures between SHF and THF. The residual temperature of parts using THF is generally higher than that of SHF due to the insulation effect of the triple-layer sheets. The lowest temperatures all occurred in area V because of a longer contacting with the blank holder and die. The highest temperatures all occur at the top. This is due to the die and the blank holder move downward together, and the sheet is under tension shown as stage II in Fig.9(b). Under the effect of the straight edge of the top surface of the punch, area I is in a suspended state without contact. In addition, at this stage, the parts of SHF come into direct contact with the punch, and the heat flows directly to the mold at this stage. There is a phenomenon of local temperature drop. However, the parts of THF did not experience

a temperature drop under the clamping effect of the steel sheet. Therefore, the titanium alloy sheet has a better plastic to be formed under THF conditions.

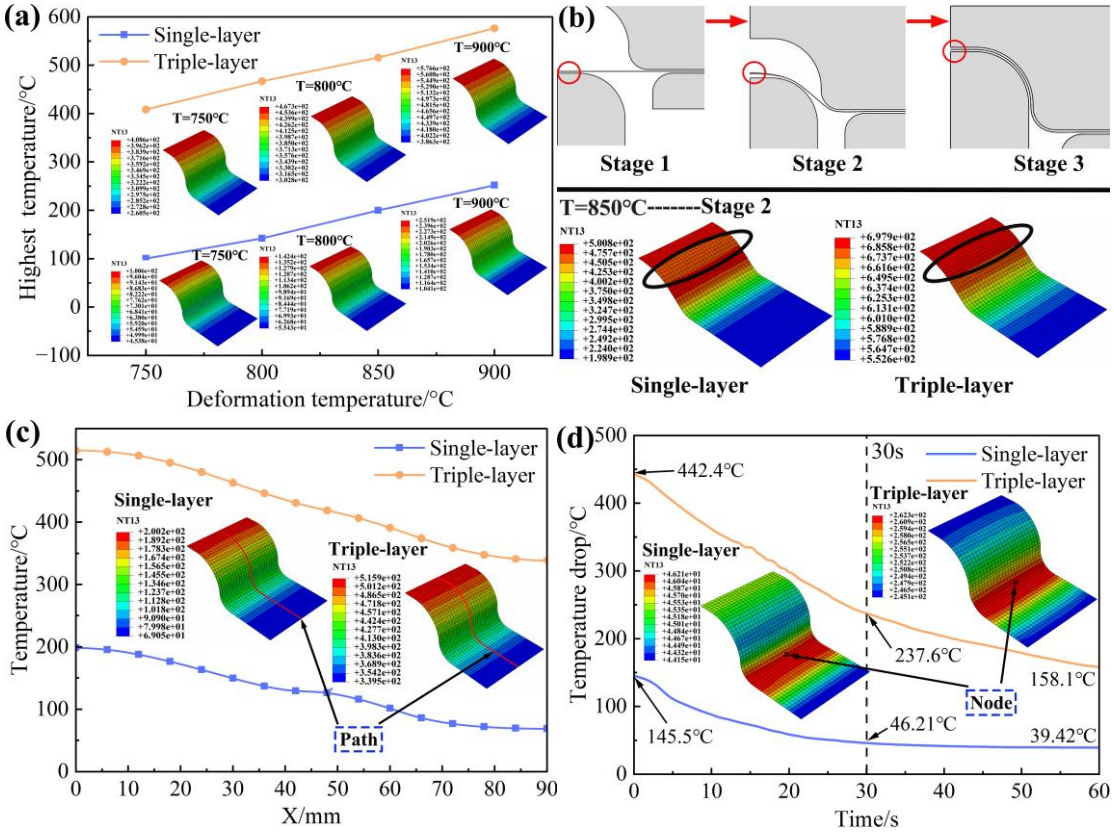


Fig.9 The temperature distribution results: (a) Temperature comparison (b) Temperature distribution changes during the forming process (c) Temperature distribution along the path after forming at 850°C (d) Temperature drop during the quenching process at 850°C

Fig.9(c) shows the temperature distribution along the path when the forming temperature is 850°C. The parts of SHF lost a considerable amount of heat, with the maximum temperature dropping from the initial 850°C to 200.2°C. The temperature in area IV is only 145.5°C. The rapid temperature dropping can cause the metastable β-phase to transform back into the α-phase, reducing the forming accuracy of the parts[32]. The highest temperature of THF is 515.9°C due to the thermal insulation effect of the steel sheet. The temperature distribution of the whole sheet is uniformed, and the maximum temperature difference is 176.4°C. The temperature in area IV still stands at 442.4°C. Fig.9(d) shows the node temperature dropping of the two processes during the quenching process. When the quenching time is 30s, the highest temperatures all

occurred in area IV, which is the same as the experimental results. The highest temperature of the parts quenched by SHF is only 46.21°C. The parts after THF quenching for 30s still have a temperature of 237.6°C. In the THF process, the pronounced SR effect will occur in area IV, which can release more residual stress during the quenching time, ultimately reducing the stress release after unloading.

4.4 SR behavior during quenching process

Fig.10 shows the stress distribution after quenching for 60s. During the quenching process, both processes exhibited varying degrees of SR behavior. In area II, the stress is large and evenly distributed. As shown in Fig.10(a), the maximum stress of the parts using THF is 98.97MPa in area III, which decreases by 64.62% comparing with the value before quenching. The stresses at the rounded corner of area II and area IV are 83.27MPa and 59.72MPa, respectively. The stress is significantly reduced compared to that after forming (Fig.7(c)). It indicates that the titanium alloy sheet undergoes a relatively significant SR behavior during the quenching process. This is the main reason for the small springback in the THF process. However, the maximum stress of the parts using SHF is 222MPa which decreases by 30.82% comparing with the value before quenching, as shown in Fig.10(b). There is still significant stress after quenching, with only a small amount of SR occurring. After unloading, it is prone to produce significant springback.

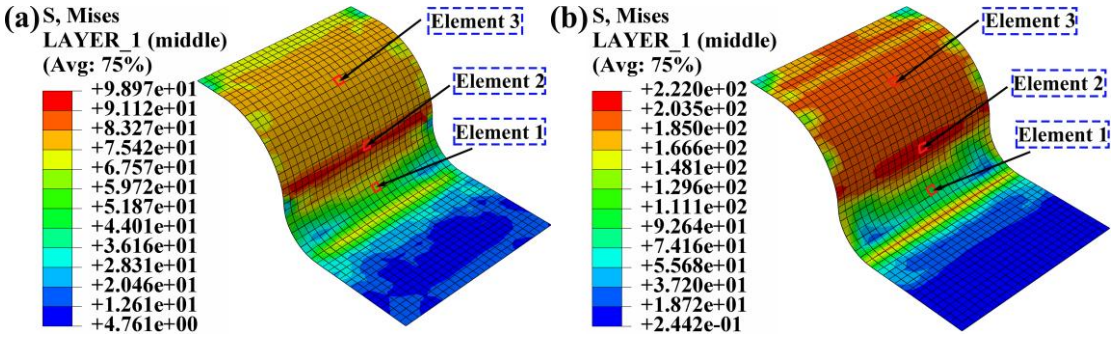


Fig.10 The stress distribution for quenching 60s at 850°C: (a) Triple-layer (b) Single-layer

The SR and creep have the same essence and can be regarded as a transient creep process[33]. The temperature at the node of THF parts remains at 158.1°C after 60s of quenching. Therefore, the quenching time is extended to 600s to observe the SR

behavior, as shown in Fig.11. In the THF process, the direction of temperature during the quenching process results in the lowest SRL of element 1. The stress from 186.6MPa of before SR to 3.2MPa of after SR for 600s, with the SR attenuation by 98.29%. Due to its proximity to the direction of temperature and the highest strain, the SR attenuation of element 2 is second only to that of element 1. The stress from 279.7MPa to 15.6MPa, with the SR attenuation by 94.42%. However, element 3 has the smallest degree of deformation and cannot provide sufficient movable dislocations for SR[34]. The stress from 163.3MPa to 27.1MPa, with the SR attenuation by 83.4%. In conclusion, the element 1 has the greatest SR attenuation, and the area IV where it is located has the most significant impact on springback. In the SHF process, the SR attenuation of the three elements after quenching for 600s is 40.6%, 55.84%, and 14.34% respectively. Among them, the attenuation magnitude of element 2 is greater than that of element 1. This is because the temperature differences between the two positions are not significant and the low temperature is not conducive to stress release. The strain of element 2 is large, and the influence of strain on SR dominates. Meanwhile, the deformation of element 3 is the least resulting in the lowest attenuation magnitude. After unloading, the springback of area II is the greatest. Compared with the results obtained by THF process, the SR attenuation magnitude of the SHF element 1 is 58.69% lower than that of the THF. The quenching time has a relatively small influence on the control of springback. Therefore, under the THF process, the springback is effectively controlled.

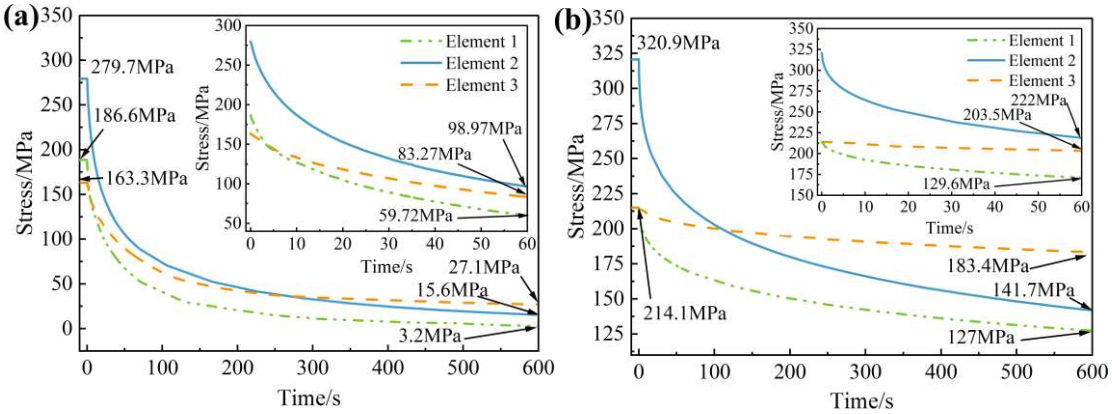


Fig.11 The SR during quenching process at 850℃: (a) Triple-layer (b) Single-layer

4.5 Strain neutral layer shift and microstructure analysis of area IV

The core feature of THF lies in the absence of adhesion between the sheets, with the load being transferred solely through mechanical contact. It mainly relies on the coupling effect of contact pressure and friction force. As shown in Fig.12(a), the inner and outer layers of TC4 alloy area IV receive deformation forces from the steel sheet during the deformation process. The outer layer of the upper steel sheet is tensioned, while the inner layer of the lower steel sheet is compressed. Therefore, under the action of the frictional force, the inner layer will be subjected to an outward tensile frictional force, which is F_X'. The outer layer of TC4 alloy will be subjected to an inward compressive frictional force, which is F_L'. In addition, under the action of the steel sheet clamping, it will not be affected by the downward friction of the die. Fig.12(b) shows the force conditions of the SHF components. The inner layer of the TC4 alloy sheet is affected by the friction force because of the contacting with the die. However, the outer layer is not affected by friction force. This results in asymmetric compressive and tensile deformation resistances between the inner and outer layers of the TC4 alloy sheet, causing a shift of the neutral layer as shown in Fig.12(c).

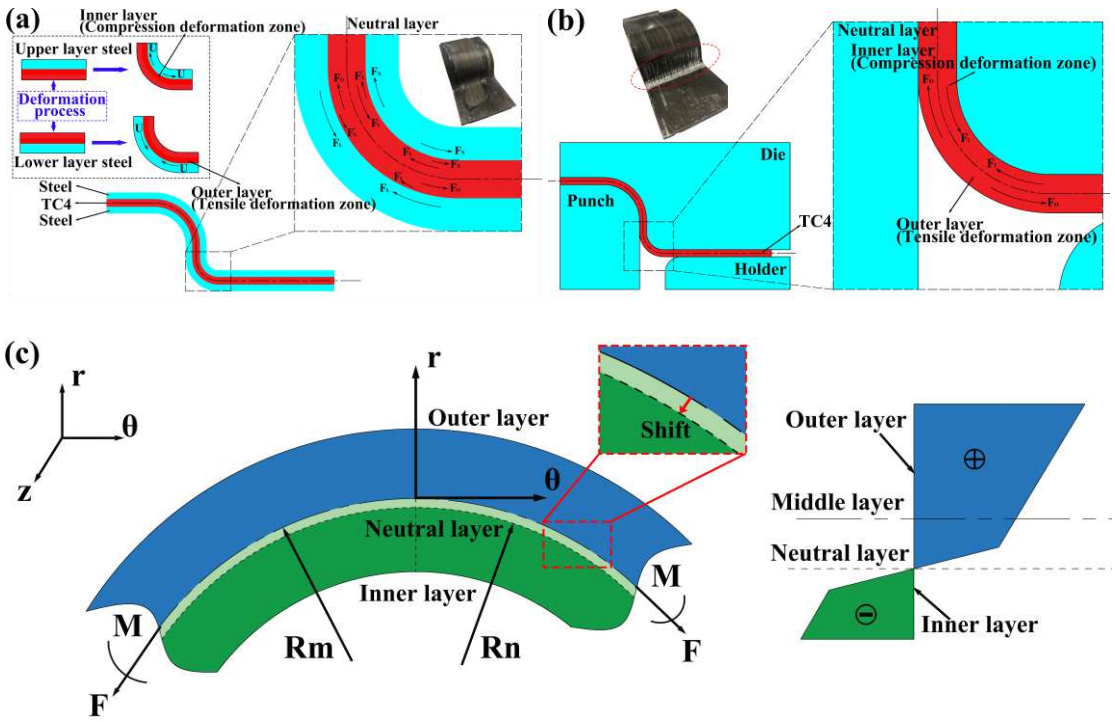


Fig.12 (a) Triple-layer theoretical mechanics analysis (b) Single-layer theoretical mechanics analysis (c) The tensile bending model

It is assumed that the thickness of the sheet material remains constant during the

bending process. Before the deformation, the position of the strain neutral layer should align with the geometric neutral layer. After deformation, the position where the tangential strain from the inner layer to the outer layer becomes zero[35]. As shown in Fig.13(a), the strain neutral layer of THF is located at 0.7347mm at 850℃. This indicates that the neutral layer has shifted towards the compression zone of the sheet material. The shift is 0.0653mm, which is less than 5% of the sheet thickness. The strain neutral layer in the SHF is located at 0.6865mm with a shift of 0.1135mm, it increased by 42.47% comparing with THF. The larger shift value expanded the effective deformation thickness of the tension zone, increases the total elastic strain in the tension zone. The springback of the part significantly increases after unloading. Fig.13(b) shows the shift of the strain neutral layer at different temperatures. As the temperature rises, both processes shift towards the compression zone, and the degree of this shift gradually weakens. The shift of SHF has decreased by 23.86%. The shift of THF decreased by 27.13%, and it is more sensitive to temperature.

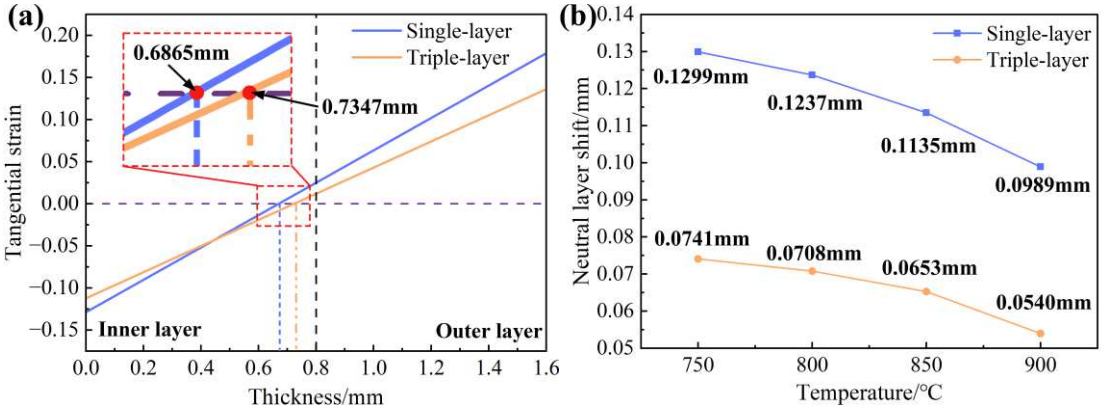


Fig.13 The strain neutral layer shift: (a) Tangential strain distribution and position of the strain neutral layer at 850℃ (b) The shift value of the strain neutral layer at different temperatures

The THF formed samples were characterized by electron backscatter diffraction (EBSD). The samples used in the analysis are the area IV of the 850°C formed parts, including the outer, middle, and inner layers. The sample size is 10×10mm, as shown in Fig.14. From the IPF view in the transverse direction (TD), three positions are composed of grains with multi-color orientations. However, there is a significant difference in the grain orientation compared to the initial microstructure. After THF,

the randomly oriented grains in the initial microstructure rotated, as shown in Fig.14(a). The main transformation is towards the [10-10] orientation, and the change in lattice orientation is mainly achieved through the activation of the columnar slip system[36]. In addition, three positions all exhibit a left-bottom to right-up striped pattern, which may be related to the complex deformation history of the U-shaped part. Fig.14(d) shows the distribution of grain sizes. It can be observed that the grain sizes are mainly distributed in the range of 1-10μm. With its unique heat retention effect, under the effect of dynamic recovery, small grains (1-2μm) coalesce and grow through grain boundary migration driven by interfacial energy at high temperatures. Meanwhile, the migration of grain boundaries causes LAGBs to gradually transform into high-angle grain boundaries (HAGBs), and the proportion of LAGBs decreases. The large grains (>10μm) are divided into smaller grains by the sub-grain boundaries formed during recrystallization, and the rate of sub-grain formation is lower than the rate of coalescence of the smaller grains. Meanwhile, the recrystallization process consumed the high-dislocation regions. This resulted in a decrease in the dislocation density of the tissue after THF treatment, as shown in Fig.14(b). In addition, the recrystallized grains reduce the original texture strength, as shown in Fig.14(c) for the {10-10}. However, this contradicts the preferential selection orientation mentioned in the previous paragraph [10-10], and this might be caused by the activation of multiple slip systems.

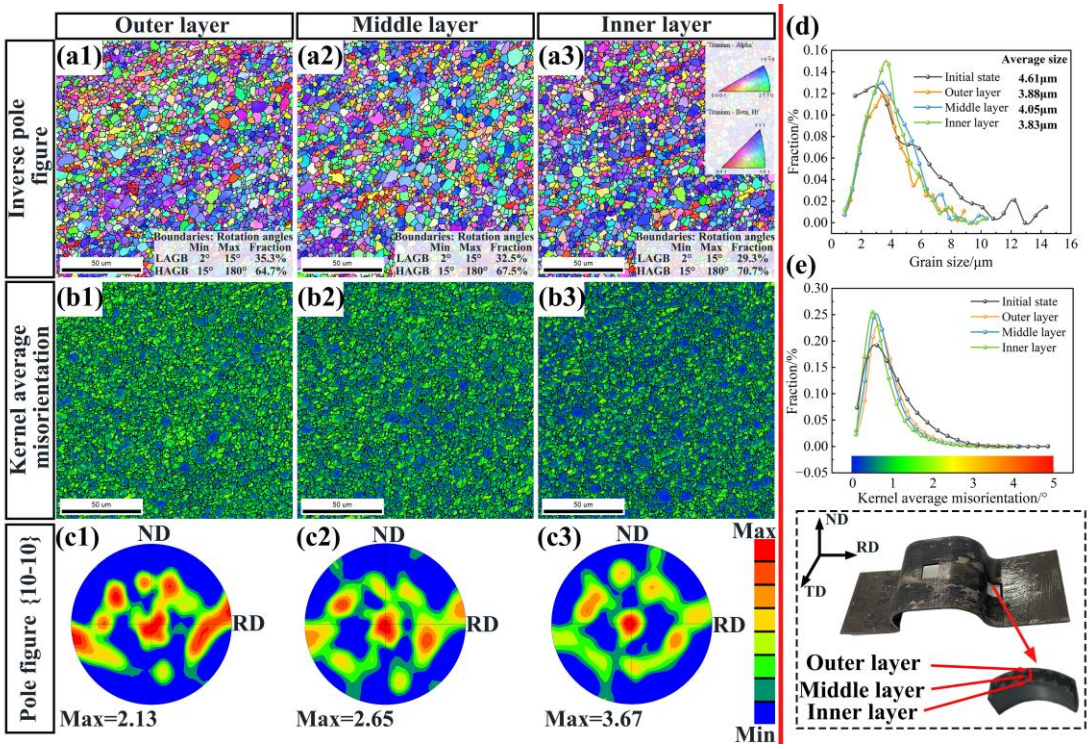


Fig.14 Microstructure evolution of area IV of the parts formed by THF at 850℃: (a1-c1) Outer layer (a2-c2) Middle layer (a3-c3) Inner layer (d) Average grain size (e) KAM distribution

In view of the asymmetry of tension and compression that exists after bending, it is necessary to study the differences between the layers of the test specimen. There are no elongated grains caused by tension zone in the tissue of outer layer from the IPF image. The average grain sizes of the outer and inner layers are and 3.88μm and 3.83μm respectively, showing no significant difference. The average grain size of the middle layer is 4.05μm, which is caused by the relatively small strain. In addition, the proportion of LAGBs in the outer layer along the normal direction (ND) decreases from 35.3% to 29.3% in the inner layer, it is reduced by only 6%. As shown in Fig.14(c) and (e), the difference in dislocations is also not significant, showing a weak decreasing trend. During the bending process, the deformation resistance in the compression zone is much greater than that in the tension zone of TC4 alloy, and it should have higher texture strength. However, the texture strength is not much difference from {10-10} of outer, middle and inner layer is 2.13, 2.65 and 3.67, respectively. The minor differences indicate that THF mitigated the tension and compression asymmetry phenomenon. Therefore, the parts of THF, due to its superior manufacturing process. After unloading,

the springback of the parts is small and uniform.

5 Application of THF

5.1 Experimental test of typical aviation titanium alloy skin parts

A typical titanium alloy aerospace skin part test is conducted. Due to the large size of this part, the dimensions of the part are adjusted, the proportion is 1/4. The adjusted dimension of the part and its tool are shown in Fig.15. The test materials and procedures are the same as those for the U-shaped part. The sheet material size is 260×140mm. Due to the large size of the parts, the quenching time needs to be extended to ensure that the stress is fully released. The quenching time is set at 150s. The test temperatures were set at 850℃, 900℃, and 950℃. The pressing speed is 30mm/s.

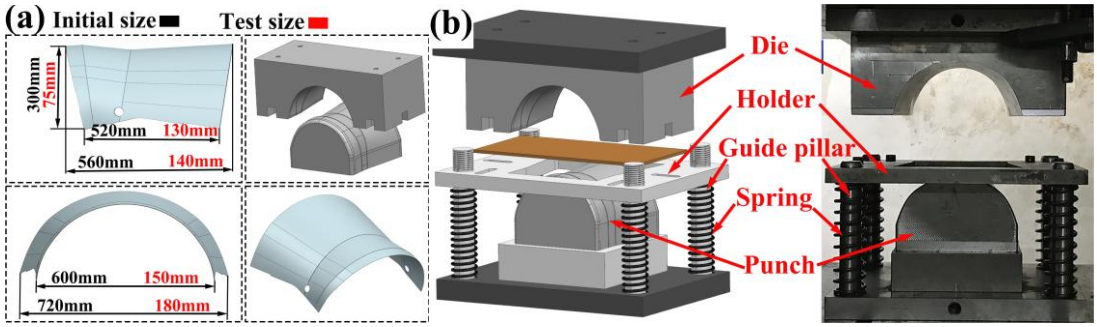


Fig.15 Aerospace skin part and tools (a) Illustration of the part's shape (b) Forming tools

5.2 Results and analysis

Fig.16(a) shows the skin parts after forming. Both processes have achieved good forming results, but there are varying degrees of springback. Due to the complexity of the parts, it is impossible to assess the springback using simple angle measurements. Therefore, a 3D scanner is used to perform a full-area scan of the skin part, which is shown in Fig.16(b).

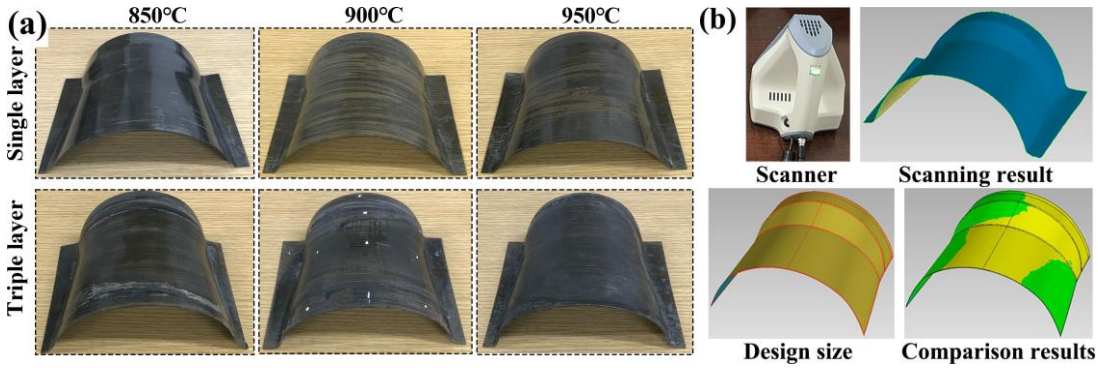
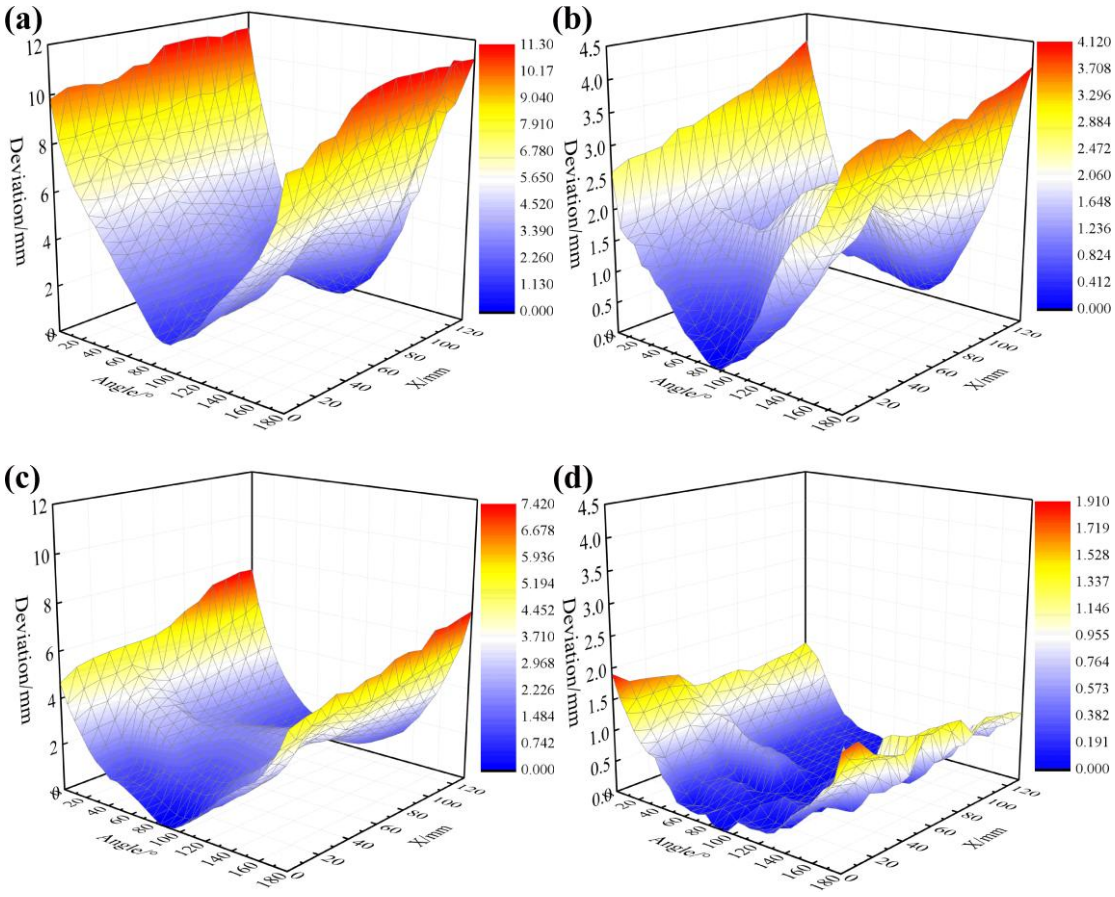


Fig.16 The forming results and scanning equipment: (a) Skin parts (b) Scanning equipment

Fig.17 shows the distribution of the deviations of the skin parts. The maximum deviation is mainly concentrated on both sides of the part and gradually decreases towards the symmetrical plane. The skin parts obtained through SHF process have significant deviations. When the temperature is 850℃, the maximum deviation is 11.3mm. When the temperature rises, the maximum deviation remains at a relatively high level of 2.78mm. However, the skin parts obtained by THF process have smaller deviations and higher precision. The maximum deviation decreased from 4.12 mm of 850℃ to 0.63 mm of 950℃. The deviation of THF from SHF decreased by 63.5% at 850℃. As the temperature rises to 950°C, the reduction is further increased to 77.3%. The effect of temperature on THF is significantly greater than that on SHF. In conclusion, THF can effectively suppress springback.



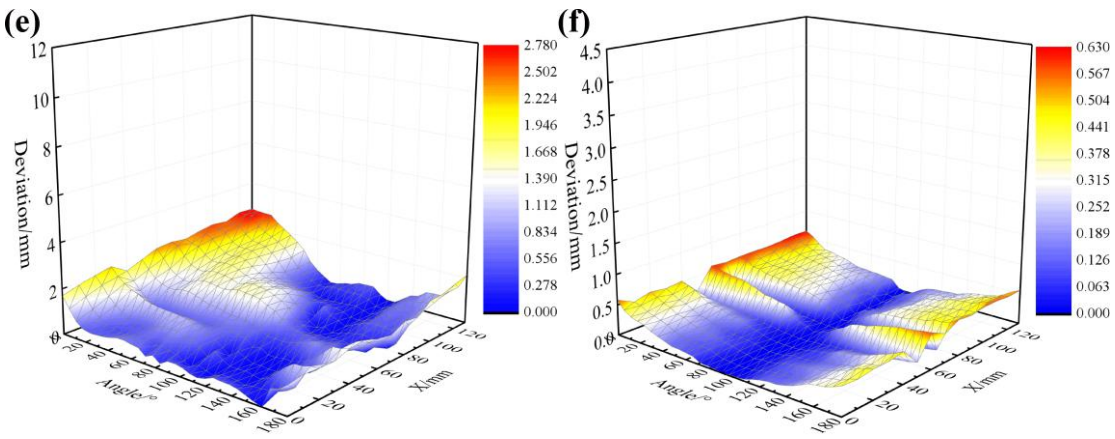
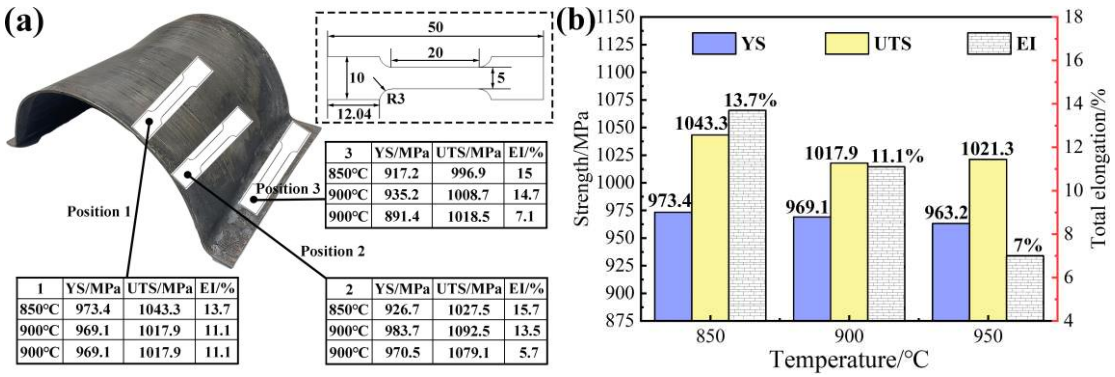


Fig.17 The deviation distribution of skin parts: Single-layer (a) 850℃ (c) 900℃ (e) 950℃; Triple-layer (b) 850℃ (d) 900℃ (f) 950℃

In order to measure the mechanical properties of the skin parts after THF treatment, uniaxial tensile tests were conducted on different positions of the THF skin parts at different forming temperatures. The positions and dimensions are shown in Fig.18(a). At 850℃, although the ultimate tensile strength (UTS) at the three positions decreased compared to 1069 MPa at room temperature. Position 3 has the lowest value, which is only 996.9 MPa. However, the elongation index (EI) of all samples has increased. The EI at position 2 is as high as 15.7%. Compared with 4.7% under room temperature increased by about 70%. When the forming temperature is 900℃, the UTS at position 2 is 1092.5 MPa and the EI is 13.5%. It has a high degree of strength and retains a high EI. At 950℃, and the EI of the materials all decreased to 7.1% or below. The UTS at position 2 is the highest, reaching 1079.1 MPa. In conclusion, although the mechanical properties at different positions of the part vary slightly at different forming temperatures, the differences are not significant. Therefore, in the THF process, better mechanical properties can be achieved.



1	YS/MPa	UTS/MPa	EI/%
850℃	973.4	1043.3	13.7
900℃	969.1	1017.9	11.1
900℃	969.1	1017.9	11.1

2	YS/MPa	UTS/MPa	EI/%
850℃	926.7	1027.5	15.7
900℃	983.7	1092.5	13.5
900℃	970.5	1079.1	5.7

3	YS/MPa	UTS/MPa	EI/%
850℃	917.2	996.9	15
900℃	935.2	1008.7	14.7
900℃	891.4	1018.5	7.1

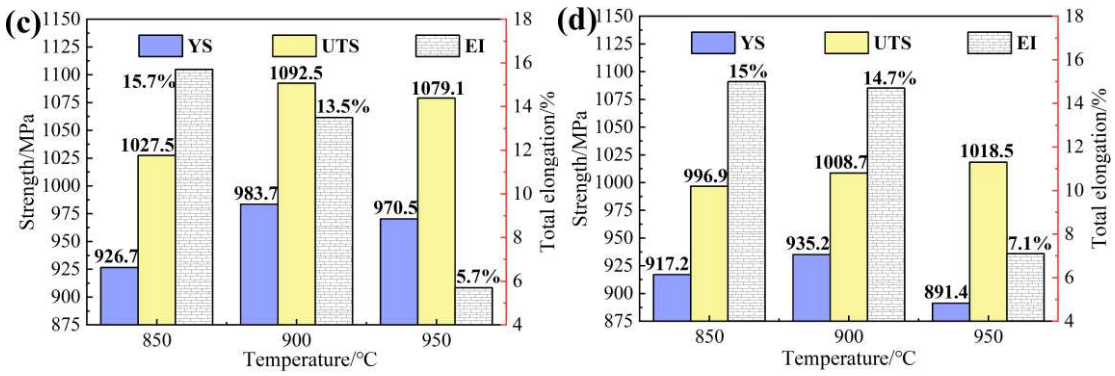


Fig.18 The uniaxial tensile properties of skin parts under different temperatures and positions: (a) Position and size of the tensile specimen; Tensile properties (b) Position 1 (c) Position 2 (d) Position 3

6 Conclusion

This paper conducts a study on the springback behavior and control ability of THF for the TC4 alloy by experiments and FE simulations. The effect of forming temperatures and quenching times on springback is studied, and the SR behavior during the quenching process is revealed. The shift of the neutral layer and the evolution of the microstructure are analyzed. Finally, typical aviation component experiments are conducted to verify the springback control of the THF process. The main conclusions are as follows:

(1) The change in springback angle is negatively correlated with sheet temperature and quenching time. The springback angle decreases from 2.67° of 750°C to 0.46° of 900°C in the THF process, which decreases by 82.78%. During the quenching stage, the springback angle decreases from 0.58° of 30s to 0.24° of 60 s, which decreases by 58.62%. The FE model has a high predictive ability with a R of 99.69%. In the areas with high stress and strain, the components exhibit the characteristics of low stress and high strain in the THF process.

(2) In the THF process, under the effect of the triple-layer sheets insulation, the residual temperature of parts is generally higher than that of SHF. The direction of temperature during the quenching process result in the lowest SRL of element 1. The stress from 186.6MPa of before SR to 3.2MPa of after SR for 600s, with the SR attenuation by 98.29%. Compared with the results obtained by SHF process, the SR attenuation magnitude of the THF element 1 is 58.69% higher than that of the SHF. It

is more significantly affected by temperature and quenching time.

(3) The strain neutral layers in both process area IV are shifted towards the compression zone. At 850℃, the shift of THF is 0.0653mm, while that of SHF is 0.1135mm. An increase in temperature will decrease the shift of the neutral layer. The microstructure difference between the inner and outer layers of THF parts is not significant, which alleviates the tension-compression asymmetry caused by sheet material bending.

(4) In application, the maximum deviation reduction of THF compared to SHF is 77.3%, and it is more significantly affected by temperature. The reliability of THF is verified through the skin experiment, and it can be applied to thin-walled parts in the aerospace field to achieve high-precision forming. Better mechanical properties can be achieved.

CrediT authorship contribution statement

Lida Yu: Conceptualization, Investigation, Methodology, Formal analysis, Data curation, Validation, Writing – original draft. **Xiaoming Yang:** Supervision, Validation, Writing – review & editing, Resources, Project administration, Funding acquisition. **Shengqiang Liu:** Investigation, Data curation. **Xiaomin Huang:** Visualization, Validation, Formal analysis. **Baoyu Wang:** Validation, Data curation. **Hongchao Ji:** Validation, Supervision.

Declaration of competing interest

The authors declare that they have no known competing financial interests or personal relationships that could have appeared to influence the work reported in this paper.

Availability of data and materials

The authors confirm that the data and materials supporting the findings of this study are available within the article.

Acknowledgments

This work was supported by the Youth Fund Project of Hebei Provincial Department of Education (Grant number: QN2024242).

References

[1] Srivastava M, Jayakumar V, Udayan Y, et al. Additive manufacturing of Titanium alloy for aerospace applications: Insights into the process, microstructure, and mechanical properties. Appl Mater Today. 2024, 41: 102481. https://doi.org/10.1016/j.apmt.2024.102481

[2] Akula SP, Ojha M, Rao KL, et al. A review on superplastic forming of Ti-6Al-4V and other titanium alloys. Mater Today Commun. 2023, 34: 105343. https://doi.org/10.1016/j.mtcomm.2023.105343

[3] Bong HJ, Yoo DH, Kim D, et al. Correlative study on plastic response and formability of Ti-6Al-4V sheets under hot forming conditions. J Manuf Process. 2020, 58: 775-786. https://doi.org/10.1016/j.jmapro.2020.08.053

[4] Badr OM, Rolfe B, Weiss M. Effect of the forming method on part shape quality in cold roll forming high strength Ti-6Al-4V sheet. J Manuf Process. 2018, 32: 513–521. https://doi.org/10.1016/j.jmapro.2018.03.022

[5] Lee JU, Hyun YT, Lim JS, et al. Effect of bending speed on springback and thinning behavior of commercially pure titanium sheets under V-bending. Mater Des. 2025: 114231. https://doi.org/10.1016/j.matdes.2025.114231

[6] Zajkani A, Hajbarati H. Investigation of the variable elastic unloading modulus coupled with nonlinear kinematic hardening in springback measuring of advanced high-strength steel in U-shaped process. J Manuf Process. 2017, 25: 391-401. https://doi.org/10.1016/j.jmapro.2016.12.022

[7] Jiang HJ, Ren YX, Lian JW, et al. A new predicting model study on U-shaped stamping springback behavior subjected to steady-state temperature field. J Manuf Process. 2022, 76: 21-33. https://doi.org/10.1016/j.jmapro.2022.02.004

[8] De Souza T, Rolfe BF. Characterising material and process variation effects on springback robustness for a semi-cylindrical sheet metal forming process. Int J Mech Sci. 2010, 52(12): 1756-1766.

https://doi.org/10.1016/j.ijmecsci.2010.09.009

[9] Chen C, Liang J, Li Y, et al. Springback analysis of flexible stretch bending of multi-point roller dies process for Y-profile under different process parameters. Metals. 2021, 11(4): 646.
https://doi.org/10.3390/met11040646

[10] Zhang H, Yu H, Zhang J, et al. Simulation and experimental investigation on bending springback of TA2/PEEK/Cf hybrid laminates with hemispherical micro-pit arrays at TA2/PEEK interfaces. Compos Commun. 2025: 102644.
https://doi.org/10.1016/j.coco.2025.102644

[11] Huang X, Guan B, Zang Y, et al. Investigation of defect behavior during the stamping of a thin-walled semicircular shell with bending angle. J Manuf Process. 2023, 87: 231-244.
https://doi.org/10.1016/j.jmapro.2023.01.026

[12] Yang X, Dang L, Wang Y, et al. Springback prediction of TC4 titanium alloy V-bending under hot stamping condition. Cent South univ. 2020, 27(9): 2578-2591.
https://doi.org/10.1007/s11771-020-4483-y

[13] Zong Y, Liu P, Guo B, et al. Springback evaluation in hot v-bending of Ti-6Al-4V alloy sheets. Int J Adv Manuf Tech. 2015, 76(1): 577-585.
https://doi.org/10.1007/s00170-014-6190-z

[14] Ao D, Chu X, Yang Y, et al. Effect of electropulsing on springback during V-bending of Ti-6Al-4V titanium alloy sheet. Int J Adv Manuf Tech. 2018, 96(9): 3197-3207.
https://doi.org/10.1007/s00170-018-1654-1

[15] Shivaprasad C, Subrahmanyam A, Reddy NV. Effect of electric path in electric pulse aided V-bending of Ti-6Al4V: an experimental and numerical study. J Manuf Process. 2023, 100: 75–84.
https://doi.org/10.1016/j.jmapro.2023.05.018

[16] Matsumoto H, Velay V. Mesoscale modeling of dynamic recrystallization behavior, grain size evolution, dislocation density, processing map characteristic, and room temperature strength of Ti-6Al-4V alloy forged in the (α+β) region. J Alloy Compd.

2017, 708: 404-413.
https://doi.org/10.1016/j.jallcom.2017.02.285

[17] Zhang T, Liu Y, Sanders DG, et al. Development of fine-grain size titanium 6Al–4V alloy sheet material for low temperature superplastic forming. Mater Sci Eng A. 2014, 608: 265-272.
https://doi.org/10.1016/j.msea.2014.04.098

[18] Barnes AJ. Superplastic forming 40 years and still growing. J Mater Eng perform. 2007, 16(4): 440-454.
https://doi.org/10.1007/s11665-007-9076-5

[19] Mosleh AO, Kotov AD, Vidal V, et al. Initial microstructure influence on Ti–Al–Mo–V alloy's superplastic deformation behavior and deformation mechanisms. Mater Sci Eng A. 2021, 802: 140626.
https://doi.org/10.1016/j.msea.2020.140626

[20] Xiang W, Xiang Y, Zhang F, et al. Study on stress relaxation and creep behavior of TB18 titanium alloy during the aging process. Mater Sci Eng A. 2024, 893: 146125.
https://doi.org/10.1016/j.msea.2024.146125

[21] Pan D, Kai Z, Xu M. Process parameters optimization of Ti-6Al-4V alloy sheet during hot stretch-creep forming. Trans Nonferrous Met Soc China. 2015, 25(2): 420-428.
https://doi.org/10.1016/S1003-6326(15)63619-6

[22] Chen C, Chen M, Xie L, et al. Numerical and experimental investigations of the hot stamping process for complex aircraft skin parts composed of TA32 high-temperature titanium alloy using an Arrhenius-type constitutive model. Int J Adv Manuf Tech. 2019, 103(1): 807-817.
https://doi.org/10.1007/s00170-019-03568-7

[23] Qu B, Zhao C, Wang K, et al. A novel integrated hot forming with in-situ stress relaxation-aging for titanium alloy thin-walled components. J Manuf Process. 2024, 131: 1296-1308.
https://doi.org/10.1016/j.jmapro.2024.09.113

[24] Yuan S, Fan X. Developments and perspectives on the precision forming processes for ultra-large size integrated components. Int J Extreme Manuf. 2019, 1(2): 022002.
https://doi.org/10.1088/2631-7990/ab22a9

[25] Liu X, Kopec M, El Fakir O, et al. Characterisation of the interfacial heat transfer coefficient in hot stamping of titanium alloys. Int Commun Heat Mass Transfer. 2020, 113: 104535.
https://doi.org/10.1016/j.icheatmasstransfer.2020.104535

[26] Kopec M, Wang K, Politis DJ, et al. Formability and microstructure evolution mechanisms of Ti6Al4V alloy during a novel hot stamping process. Mater Sci Eng A. 2018, 719: 72-81.
https://doi.org/10.1016/j.msea.2018.02.038

[27] Yang X, Wang B, Zhou J. Numerical and experimental study on formability of TC4 alloy in a novel multi-layer sheet hot stamping process. Int J Adv Manuf Tech. 2020, 110(5): 1233-1247.
https://doi.org/10.1007/s00170-020-05802-z

[28] Zhou J, Yang X, Wang B, et al. Investigation of interfacial heat transfer characterization for TC4 alloy in triple-layer sheet hot stamping process. Int J Adv Manuf Tech. 2022, 121(9): 5779-5792.
https://doi.org/10.21203/rs.3.rs-1507276/v1

[29] Lang L, Danckert J, Nielsen KB. Multi-layer sheet hydroforming: Experimental and numerical investigation into the very thin layer in the middle. J Mater Process Technol. 2005, 170(3): 524-535.
https://doi.org/10.1016/j.jmatprotec.2005.06.033

[30] Mu Y, Yang X, Wang B, et al. A novel triple-layer hot stamping process of titanium alloy TC4 sheet for enhancing formability and its application in a plug socket part. Int J Lightweight Mater Manuf. 2023, 6(2): 189-197.
https://doi.org/10.1016/j.ijlmm.2022.10.003

[31] Sun W, Yang X, Liu S, et al. Thermal deformation behavior and constitutive model of TC4 titanium alloys at hot tensile process. Mate Today Commun. 2025, 113618.

https://doi.org/10.1016/j.mtcomm.2025.113618

[32] Zheng K, Li D, Chen H, et al. Effect of cooling rate on the phase transformation and post strength of Ti-6Al-4V under hot forming conditions: Experiments and modelling. J Alloy Compd. 2024, 972: 172868.
https://doi.org/10.1016/j.jallcom.2023.172868

[33] Peng H, Hou Z, Chen X, et al. Effect of temperature and cyclic loading on stress relaxation behavior of Ti–6Al–4V titanium alloy. Mater Sci Eng A. 2021, 824: 141789.
https://doi.org/10.1016/j.msea.2021.141789

[34] Luo J, Xiong W, Li X, et al. Investigation on high-temperature stress relaxation behavior of Ti-6Al-4V sheet. Mater Sci Eng A. 2019, 743: 755-763.
https://doi.org/10.1016/j.msea.2018.11.151

[35] Xia L, Xu Y, Xie W, et al. A novel strategy for reducing sheet springback by coupled with high strain rate and shear deformation via impact hydroforming. J Manuf Process. 2024, 132: 392-403.
https://doi.org/10.1016/j.jmapro.2024.10.076

[36] Fan J, Chen Z, Zhao D, et al. Temperature-Dependent Crack Behavior and Microstructure Evolution Mechanisms in Hot Stamped Ti65 Titanium Alloy Sheets. J Alloy Compd. 2025: 182482.
https://doi.org/10.1016/j.jallcom.2025.182482